

# Two-color QCD at imaginary chemical potential and its impact on real chemical potential

Kouji Kashiwa,<sup>1</sup> Takahiro Sasaki,<sup>2</sup> Hiroaki Kouno,<sup>3</sup> and Masanobu Yahiro<sup>2</sup>

<sup>1</sup>*RIKEN/BNL Research Center, Brookhaven National Laboratory, Upton, NY-11973, USA*

<sup>2</sup>*Department of Physics, Graduate School of Sciences, Kyushu University, Fukuoka 812-8581, Japan*

<sup>3</sup>*Department of Physics, Saga University, Saga 840-8502, Japan*

(Dated: January 13, 2019)

We study properties of two-color QCD at imaginary chemical potential ( $\mu$ ) from the view point of the Roberge-Weiss (RW) periodicity, the charge conjugation and the pseudo-reality. At  $\mu = i\pi T/2$ , where  $T$  is temperature, the system has both the  $\mathbb{Z}_2$  and the charge-conjugation symmetry. The two symmetries are preserved at lower  $T$ , but simultaneously broken at higher  $T$ . The Polyakov-loop extended Nambu–Jona-Lasinio (PNJL) model has the same properties as two-color QCD for the RW periodicity, the charge conjugation and the pseudo-reality. The nontrivial correlation between the chiral and  $\mathbb{Z}_2$  symmetry breakings are investigated by introducing the entanglement vertex in the PNJL model. The order of the  $\mathbb{Z}_2$  symmetry breaking at the RW endpoint is the second order when the correlation is weak, but becomes the first order when the correlation is strong. We also investigate the impact of the correlation on the phase diagram at real  $\mu$ .

PACS numbers: 11.30.Rd, 12.40.-y, 21.65.Qr, 25.75.Nq

## I. INTRODUCTION

Elucidation of QCD at finite temperature ( $T$ ) and finite quark-number chemical potential ( $\mu$ ) is one of the most important subjects in hadron physics. Lattice QCD (LQCD) is the first-principle calculation, but has the sign problem at real  $\mu$ . Particularly at  $\mu/T \gtrsim 1$ , the LQCD calculation is not feasible, although several methods have been proposed so far to circumvent the problem; see for example Ref. [1]. For this reason, effective models such as the Polyakov-loop extended Nambu–Jona-Lasinio (PNJL) model [2–6] are widely used to investigate QCD at finite  $\mu$ .

Symmetries are important to understand QCD. In this paper we focus our discussion on global symmetries. QCD has the chiral symmetry in the limit of zero current quark mass ( $m$ ) and the  $\mathbb{Z}_{N_c}$  symmetry in the limit of infinite  $m$ , where  $N_c$  is the number of colors. The charge conjugation ( $\mathcal{C}$ ) symmetry is preserved at  $\mu = 0$ , but not at finite  $\mu$ . The QCD partition function  $Z(\mu)$  is, however, invariant under the combination of the charge conjugation and the parameter transformation  $\mu \rightarrow -\mu$ . This leads to a relation between  $Z(\mu)$  and  $Z(-\mu)$ :

$$Z(\mu) = Z(-\mu). \quad (1)$$

The  $\mathbb{Z}_{N_c}$  symmetry is broken explicitly for light quarks of our interest, but it plays an important role at imaginary chemical potential  $\mu = i\theta T$ , where  $\theta$  is the dimensionless imaginary chemical potential. The QCD partition function  $Z(\theta)$  is not invariant under the  $\mathbb{Z}_{N_c}$  transformation

$$q \rightarrow Uq, \quad A_\nu \rightarrow UA_\nu U^{-1} - i(\partial_\nu U)U^{-1}, \quad (2)$$

where  $q$  is the quark field,  $A_\nu$  is the gauge field and  $U(x, \tau)$  are elements of  $SU(N_c)$  with the boundary condition  $U(x, \beta = 1/T) = \exp(2i\pi k/N_c)U(x, 0)$  for integers

$k$  from 1 to  $N_c - 1$ . However,  $Z(\theta)$  is invariant under the combination of the  $\mathbb{Z}_{N_c}$  transformation and the parameter transformation  $\theta \rightarrow \theta + 2\pi k/N_c$ , i.e., under the extended  $\mathbb{Z}_{N_c}$  transformation [4]

$$q \rightarrow Uq, \quad A_\nu \rightarrow UA_\nu U^{-1} - i(\partial_\nu U)U^{-1}, \quad \theta \rightarrow \theta + \frac{2\pi k}{N_c}. \quad (3)$$

This means that

$$Z(\theta) = Z(\theta + 2\pi k/N_c). \quad (4)$$

The relation (4) is called the Roberge-Weiss (RW) periodicity [7]. QCD at finite  $\theta$  is governed by the RW periodicity [4, 7].

The partition function  $Z(\theta)$  is  $\theta$ -even because of (1). This  $\theta$ -evenness and the RW periodicity yield a constrain on  $\theta$  as  $0 \leq \theta \leq \pi/N_c$  and hence on  $\mu^2$  as

$$\mu^2 \geq -(T\pi/N_c)^2. \quad (5)$$

At the lower bound  $\mu^2 = -(T\pi/N_c)^2$ , i.e. at  $\theta = \pi/N_c$ , the charge conjugation comes back to a symmetry. In fact,  $Z(\pi/N_c)$  is changed into  $Z(-\pi/N_c)$  by the charge conjugation, but  $Z(-\pi/N_c)$  is identical with  $Z(\pi/N_c)$  because of the RW periodicity (4). This is true for any  $N_c$ .

The  $\mathbb{Z}_{N_c}$  transformation, meanwhile, becomes a symmetry at  $\theta = \pi/N_c$ , only when  $N_c = 2$ . In the case of  $N_c = 2$ , the  $\mathbb{Z}_2$  transformation changes  $Z(\pi/2)$  into  $Z(\pi/2 \pm \pi)$ , but  $Z(\pi/2 \pm \pi)$  is identical with  $Z(\pi/2)$  owing to the charge conjugation (1). This is not the case for  $N_c \geq 3$ . For example in case of  $N_c = 3$ , the  $\mathbb{Z}_3$  transformation changes  $Z(\pi/3)$  into  $Z(\pi/3 - 2\pi k/3)$ . The partition function  $Z(\pi/3 - 2\pi k/3)$  is transformed back to  $Z(\pi/3)$  by the charge conjugation when  $k = 1$ , but not when  $k = 2$ . At the lower bound  $\mu^2 = -(T\pi/N_c)^2$ , QCD thus possesses both the  $\mathcal{C}$  and the  $\mathbb{Z}_{N_c}$  symmetry when  $N_c = 2$ , but has only the  $\mathcal{C}$  symmetry when  $N_c \geq 3$ .

At the lower bound  $\mu^2 = -(T\pi/N_c)^2$ , a first-order phase transition takes place for any  $N_c$  [7]. The transition is induced by the spontaneous breaking of the  $\mathcal{C}$  symmetry [8]. The transition is now called the RW phase transition. A current topic on the RW phase transition is the order at the endpoint. Recent three-color LQCD simulations show that the order is the first-order for small and large  $m$ , but the second-order for intermediate  $m$  [9–12]. The order may be the first-order for both two-flavor [9, 10] and three-flavor cases [11, 12], when the pion mass  $m_\pi$  has the physical value. If the order is the first-order, the RW endpoint becomes a triple-point at which three first-order transition lines meet. The PNJL model reproduces these results [13–15].

Two-color QCD has some interesting points. The number of colors,  $N_c$ , can vary from 2 to infinity, that is, realistic three-color QCD is between two-color QCD and large  $N_c$  QCD. In this sense, understanding of both two-color and large  $N_c$  QCD is important. The algebraic approach based on the pseudo-reality [16] plays an important role in two-color QCD, while large  $N_c$  QCD is well understood by the geometric approach based on the  $1/N_c$  expansion [17] or the AdS/CFT correspondence [18]. In virtue of the pseudo-reality, two-color LQCD has no sign problem not only at imaginary  $\mu$  but also at real  $\mu$  [19], and consequently LQCD data are available there [20–25]. Furthermore, two-color LQCD has higher symmetries at  $\mu = iT\pi/2$ , as mentioned above.

In this paper, we study properties of two-color QCD at imaginary  $\mu$  from the view point of by the RW periodicity, the charge conjugation and the pseudo-reality. Particularly, we clarify the relation between the  $\mathbb{Z}_2$  and  $\mathcal{C}$  symmetries at  $\theta = \pi/2$ . The PNJL model has the same properties as two-color QCD for the RW periodicity, the charge conjugation and the pseudo-reality. The PNJL model is then used to investigate two-color QCD concretely. Particularly, the nontrivial correlation between the chiral and  $\mathbb{Z}_2$  symmetry breakings are investigated. In the model approach, we mainly consider the two-flavor ( $N_f = 2$ ) case.

This paper is organized as follows. In Sec. II, some properties of two-color QCD are derived by using the RW periodicity, the charge conjugation and the pseudo-reality. In Sec. III, the two-color PNJL model is formulated with the mean-field approximation. Numerical results are shown in Sec. IV. Section V is devoted to summary.

## II. PROPERTIES OF TWO-COLOR QCD

We consider the case of  $N_f = 1$  for simplicity and assume that  $\mu$  is either real or pure imaginary. The partition function  $Z$  of two-color QCD is obtained in Euclidean spacetime as

$$Z = \int DA \det[M(\mu)] \exp\left[-\frac{1}{4g^2} F_{\mu\nu}^2\right] \quad (6)$$

with

$$M(\mu) = D + m - \gamma_4 \mu, \quad (7)$$

where the Dirac operator  $D$  is defined by  $D = \gamma_\mu(\partial_\mu - iA_\mu)$  for the current quark mass  $m$  and the gauge field  $A_\nu$ , and  $F_{\mu\nu} = \partial_\mu A_\nu - \partial_\nu A_\mu - i[A_\mu, A_\nu]$ . For later convenience, we define Pauli matrices  $t_i$  in color space and the Dirac charge-conjugation matrix  $C = \gamma_2 \gamma_4$ .

The fermion determinant  $\det[M(\mu)]$  satisfies

$$(\det[M(\mu)])^* = \det[M(-\mu^*)], \quad (8)$$

since

$$\begin{aligned} (\det[M(\mu)])^* &= \det[M(\mu)^\dagger] = \det[\gamma_5 M(\mu)^\dagger \gamma_5] \\ &= \det[M(-\mu^*)]. \end{aligned} \quad (9)$$

The relation (8) indicates that  $\det[M(\mu)]$  is real when  $\mu$  is pure imaginary. The relation (8) is true for any  $N_c$ .

Two-color QCD has the pseudo-reality [16],

$$Dt_2 C \gamma_5 = t_2 C \gamma_5 D^*, \quad (10)$$

and hence the fermion determinant satisfies

$$\begin{aligned} \det[M(\mu)] &= \det[(t_2 C \gamma_5)^{-1} M(\mu) (t_2 C \gamma_5)] \\ &= (\det[M(\mu^*)])^* \end{aligned} \quad (11)$$

in virtue of the pseudo-reality (10). This means that  $\det[M(\mu)]$  is real when  $\mu$  is real. Two-color LQCD thus has no sign problem at both real and pure imaginary  $\mu$  [19]. The charge-conjugation relation (1) is obtained from (8) and (11).

The Polyakov loop  $\Phi$  is the vacuum expectation value of the Polyakov-loop operator

$$L = \frac{1}{N_c} \text{tr}_c \left( \mathcal{P} \exp \left[ i \int_0^{1/T} d\tau A_4 \right] \right). \quad (12)$$

with the time-ordering operator  $\mathcal{P}$ . The operator  $L$  is real, because

$$L^* = \frac{1}{N_c} \text{tr}_c \left( \mathcal{P} \exp \left[ -i \int_0^{1/T} d\tau (A_4)^* \right] \right) = L, \quad (13)$$

where the second equality is obtained from the identity  $t_2 A_\nu t_2 = -(A_\nu)^T = -(A_\nu)^*$ .

The Polyakov loop  $\Phi$  is then real at both real and pure imaginary  $\mu$ ; note that  $\det[M(\mu)]$  is real there. Under the charge conjugation, the factor  $-(A_4)^T$  is transformed into  $A_4$ , and hence the second equality of (13) means that  $L$  is  $\mathcal{C}$ -invariant. Using this property and the relation (1), one can see that

$$\Phi(\mu) = \Phi(-\mu). \quad (14)$$

For pure imaginary chemical potential  $\mu = iT\theta$ , it is convenient to introduce the modified Polyakov loop

$$\Psi(\theta) \equiv \Phi(\theta) e^{i\theta}. \quad (15)$$

The modified Polyakov loop satisfies the RW periodicity

$$\Psi(\theta) = \Psi(\theta + \pi), \quad (16)$$

since it is invariant under the extended  $\mathbb{Z}_N$  transformation [4]. It also satisfies

$$\Psi(\theta)^* = \Psi(-\theta) \quad (17)$$

because of (14) and the realness of  $\Phi$ . At  $\theta = \pi/N_c = \pi/2$ , both the  $\mathbb{Z}_2$  and  $\mathcal{C}$  transformations become symmetries, as mentioned in Sec. I. The order parameter of the  $\mathcal{C}$  symmetry is a  $\mathcal{C}$ -odd quantity. The relation (17) indicates that the imaginary part  $\text{Im}[\Psi(\theta)]$  is  $\mathcal{C}$ -odd ( $\theta$ -odd) and hence an order parameter of the  $\mathcal{C}$  symmetry [8]. Meanwhile, the order parameter of the  $\mathbb{Z}_2$  symmetry is  $\Phi$ . At  $\theta = \pi/2$  the two order parameters are identical, since  $\text{Im}[\Psi(\theta)] = \Phi(\theta) \sin(\theta) = \Phi(\theta)$ . This indicates that the spontaneous breakings of  $\mathbb{Z}_2$  and  $\mathcal{C}$  symmetries take place simultaneously.

Two-color LQCD simulations were made in Ref. [20, 21, 23, 25] for the  $N_f = 8$  case. The LQCD results at  $\theta = \pi/2$  show that  $\Phi = 0$  at small  $T$  but finite at large  $T$ . This indicates that the spontaneous and simultaneous breaking of  $\mathbb{Z}_2$  and  $\mathcal{C}$  symmetries occurs at some temperature  $T_c$ . Further analyses are made in Secs. III and IV by using the PNJL model.

For the  $N_f = 2$  case, the fermion determinant is described by

$$\det[M(\mu)] = \det[M_u(\mu)] \det[M_d(\mu)], \quad (18)$$

where  $\det[M_u(\mu)]$  and  $\det[M_d(\mu)]$  are the fermion determinants for u- and d-quark. Using the operator  $Ct_2$  only for  $\det[M_d(\mu)]$ , one can get the relation

$$\begin{aligned} \det[M(\mu)] &= \det[M_u(\mu)] \det[(Ct_2)^{-1} M_d(\mu) (Ct_2)] \\ &= \det[M_u(\mu)] \det[M_d(-\mu)]. \end{aligned} \quad (19)$$

This relation indicates that the  $1+1$  system with finite  $\mu$  is identical with the  $1+1^*$  system with the same amount of isospin chemical potential  $\mu_{iso}$ . Hence,  $\mu_{iso}^2$  also has a lower bound

$$\mu_{iso}^2 \geq -(T\pi/2)^2. \quad (20)$$

The diquark condensate in the former system corresponds to the pion condensate in the latter system. Because of this symmetry, we consider the former system only in the present paper.

### III. PNJL MODEL

We consider the  $N_c = N_f = 2$  case. The PNJL Lagrangian for the case is obtained by

$$\begin{aligned} \mathcal{L} &= \bar{q}(i\gamma_\nu D_\nu - m)q \\ &+ G[(\bar{q}q)^2 + (\bar{q}i\gamma_5\vec{\tau}q)^2 + |q^T Ci\gamma_5\tau_2 t_2 q|^2] \\ &- G_v(\bar{q}\gamma^\mu q)^2 + \mathcal{U}(\Phi), \end{aligned} \quad (21)$$

where  $q$  is the two-flavor quark field,  $m$  is the current quark mass and  $t_i$  and  $\tau_i$  are Pauli matrices in color and flavor spaces, respectively. In the limit of  $m = \mu = 0$ , two-color QCD has the Pauli-Gürsey symmetry [26, 27], so the PNJL Lagrangian is so constructed as to have the symmetry. Note that the vector-type four-quark interaction  $(\bar{q}\gamma^\mu q)^2$  does not work at  $\mu = 0$  in the mean-field level, since the vector-type condensate is zero at  $\mu = 0$ . The potential  $\mathcal{U}$  is a function of the Polyakov loop  $\Phi$  and the explicit form is shown later in Sec. IV.

Using the mean-field approximation, one can get the thermodynamical potential  $\Omega$  as [28]

$$\begin{aligned} \Omega &= -2N_f \int \frac{d^3p}{(2\pi)^3} \sum_{\pm} \left[ \frac{1}{2} N_c E_p^\pm + T(\ln f^- + \ln f^+) \right] \\ &+ U + \mathcal{U}(\Phi) \end{aligned} \quad (22)$$

with

$$f^\pm = 1 + 2\Phi e^{-\beta E_p^\pm} + e^{-2\beta E_p^\pm}, \quad (23)$$

$$U = G(\sigma^2 + \Delta^2) - G_v n_q^2 \quad (24)$$

for the chiral condensate  $\sigma = \langle \bar{q}q \rangle$ , the diquark condensate  $\Delta = |\langle q^T Ci\gamma_5\tau_2 t_2 q \rangle|$  and the vector condensate (quark number density)  $n_q = \langle q^\dagger q \rangle$ . Here the factors  $E_p^\pm$  are defined by

$$E_p^\pm = \text{sgn}(E_p \pm \mu_v) \sqrt{(E_p \pm \mu_v)^2 + (2G\Delta)^2}, \quad (25)$$

for finite  $\Delta$  and

$$E_p^\pm = E_p \pm \mu_v \quad (26)$$

for  $\Delta = 0$ , where  $\text{sgn}(E_p \pm \mu_v)$  is the sign function,  $E_p = \sqrt{p^2 + M^2}$ ,  $M = m - 2G\sigma$  and  $\mu_v = \mu - 2G_v n_q$ . In the limit of  $m = \mu = 0$ , the condensate  $n_q$  is zero, so that  $\Omega$  becomes invariant under the rotation in the  $\sigma$ - $\Delta$  plane as a consequence of the Pauli-Gürsey symmetry.

In the Polyakov gauge, the Polyakov-loop  $\Phi$  is obtained by

$$\Phi = \frac{1}{2} (e^{i\phi} + e^{-i\phi}) = \cos(\phi) \quad (27)$$

for real number  $\phi$ , indicating that  $\Phi$  is real. The mean fields  $X = \sigma, \Delta, n_q, \Phi$  are determined from the stationary conditions

$$\frac{\partial \Omega}{\partial X} = 0, \quad (28)$$

where  $\Omega$  is regularized by the three-dimensional momentum cutoff

$$\int \frac{d^3p}{(2\pi)^3} \rightarrow \frac{1}{2\pi^2} \int_0^\Lambda dp p^2, \quad (29)$$

because this model is nonrenormalizable.

At imaginary chemical potential  $\mu = i\theta T$ ,  $\Omega$  is invariant under the extended  $\mathbb{Z}_2$  transformation

$$\Phi \rightarrow e^{-i\pi} \Phi, \quad \theta \rightarrow \theta + \pi. \quad (30)$$

This can be understood easily by introducing the modified Polyakov-loop  $\Psi = e^{i\theta}\Phi$  and its conjugate  $\Psi^* = e^{-i\theta}\Phi$  invariant under the extended  $\mathbb{Z}_2$  transformation. The condensate  $\Delta$  is zero at imaginary  $\mu$ , since  $\Delta$  becomes finite only for  $\mu^2 \geq m_\pi^2/4$  [13, 16]. When  $\Delta = 0$ ,  $\Omega$  is rewritten into the form of (22) with

$$f^+ = 1 + 2\Psi e^{-2i\theta} e^{-\beta(E_p - 2G_v n_q)} + e^{-2\beta E_p^+}, \quad (31)$$

$$f^- = 1 + 2\Psi^* e^{2i\theta} e^{-\beta(E_p + 2G_v n_q)} + e^{-2\beta E_p^-}. \quad (32)$$

Obviously, Eqs. (31) and (32) show that  $\Omega$  is invariant under the extended  $\mathbb{Z}_2$  transformation and at the same time that  $\Omega$  has a periodicity of  $\pi$  in  $\theta$ , i.e., the RW periodicity

$$\Omega(\theta) = \Omega(\theta + \pi). \quad (33)$$

It should be noted that if  $\Delta$  is finite,  $\Omega$  will not have the RW periodicity. Since  $\theta$ -dependence of mean fields  $X = \sigma, n_q, \Psi$  are determined from  $\Omega$  by the stationary conditions (28), all the  $X$  have the RW periodicity

$$X(\theta) = X(\theta + \pi). \quad (34)$$

Furthermore, the RW periodicity  $\Psi(\theta) = \Psi(\theta + \pi)$  yields the relation

$$\Phi(\theta) = -\Phi(\theta + \pi). \quad (35)$$

We refer the relation (34) as to  $\mathbb{Z}_2$ -even and the relation (35) as to  $\mathbb{Z}_2$ -odd in this paper.

The PNJL Lagrangian  $\mathcal{L}$  is invariant under the combination of the  $\mathcal{C}$  and the parameter transformation  $\theta \rightarrow -\theta$ . This property guarantees that  $\Omega(\theta) = \Omega(-\theta)$  and shows that  $\theta$  behaves as a  $\mathcal{C}$ -odd quantity. Namely,  $\mathcal{C}$ -even quantities such as  $\sigma$ ,  $\Delta$  and  $\Phi$  are  $\theta$ -even, whereas  $\mathcal{C}$ -odd condensates such as  $n_q$  are  $\theta$ -odd. In the PNJL Lagrangian,  $\theta$  appears only through the pure imaginary factor  $i\theta$ . This shows that  $\theta$ -odd quantities become pure imaginary, while  $\theta$ -even quantities become real. The relation (17) is obtainable from the fact that  $\Phi(\theta)$  is real, because

$$\Psi(\theta)^* = (\Phi(\theta)e^{i\theta})^* = \Phi(-\theta)e^{-i\theta} = \Psi(-\theta). \quad (36)$$

The PNJL model thus has the same properties as two-color QCD for the RW periodicity and the  $\theta$ -parity.

The Polyakov-loop  $\Phi$  is  $\theta$ -even and  $\mathbb{Z}_2$ -odd. This indicates that

$$\Phi(\theta) = -\Phi(\pi - \theta) \quad (37)$$

and then  $\Phi(\theta) = 0$  at  $\theta = \pi/2$ , if  $\Phi$  is a smooth function of  $\theta$ . When  $T$  is larger than some temperature  $T_c$ ,  $\Omega$  is not a smooth function of  $\theta$  at  $\theta = \pi/2$ . This is the RW phase transition. Once the RW phase transition occurs,  $\Phi(\theta)$  is not smooth at  $\theta = \pi/2$  and consequently  $\Phi(\theta)$  becomes finite there. This means that the spontaneous breaking of  $\mathbb{Z}_2$  symmetry is induced by the RW phase transition. The relation (36), meanwhile, indicates that

$\text{Im}[\Psi]$  is  $\theta$ -odd ( $\mathcal{C}$ -odd) and then an order parameter of the  $\mathcal{C}$  symmetry. The fact that  $\text{Im}[\Psi]$  is  $\theta$ -odd and  $\mathbb{Z}_2$ -even leads to the same relation

$$\text{Im}[\Psi(\theta)] = -\text{Im}[\Psi(\pi - \theta)] \quad (38)$$

as (37). Both the  $\mathbb{Z}_2$  and the  $\mathcal{C}$  symmetry are thus broken spontaneously by the RW phase transition, so that the two spontaneous breakings take place simultaneously.

## IV. NUMERICAL RESULTS

### A. Parameter setting

For the  $N_c = N_f = 2$  case, we do not have enough LQCD data at imaginary chemical potential. We then make qualitative analyses here. It is well known from the nonlocal version of the PNJL model [5, 6, 29, 30] that there is the correlation between the chiral order-parameter and the Polyakov-loop in the coupling constant through the distribution function. This feature can be phenomenologically introduced in the local PNJL model by using the entanglement vertex [14]. This entanglement is taken into account in the present analysis. We make the following parameter setting.

1. Since the ratio  $r \equiv G_v/G$  is of order  $(N_c)^0$  in the leading order of the  $1/N_c$  expansion, we take  $r = 0.4$  that is determined from the  $N_c = 3$  case by comparing the result of the nonlocal PNJL model with LQCD data at finite imaginary chemical potential.
2. We introduce the entanglement vertex of the form  $G_i(1 - \alpha\Phi^2)$  for  $G_i = G$  and  $G_v$ , respecting the  $\mathbb{Z}_2$  symmetry. Here the entanglement parameter  $\alpha$  is treated as a free parameter, but is assumed to be common for both  $G$  and  $G_v$ . We mainly use  $\alpha = 0.4$  at which pseudo-critical temperatures of the chiral and deconfinement transitions almost coincide when  $\mu = 0$ .
3. In the leading order of the  $1/N_c$  expansion,  $m_\pi$  is scaled by  $(N_c)^0$  and the pion decay constant  $f_\pi$  by  $\sqrt{N_c}$ . These scaling properties are assumed to determine the parameters  $G$ ,  $\Lambda$  and  $m$  of the NJL sector, where  $m$  is simply assumed to be 5.4 MeV. In this parameter set, the dynamical quark mass  $M$  becomes  $M_0 = 305$  MeV at  $T = \mu = 0$ . The resulting parameters are shown in Table I, together with the values of  $m_\pi$ ,  $f_\pi$  and  $M_0$ .
4. Following Ref. [28], we take the Polyakov-loop effective potential of the form

$$\frac{\mathcal{U}(\Phi)}{T} = -b \left[ 24e^{-a/T} \Phi^2 + \ln(1 - \Phi^2) \right] \quad (39)$$

with  $a = 858.1$  MeV and  $b^{1/3} = 210.5$  MeV. This potential yields a second-order deconfinement transition in the pure gauge limit.

The Polyakov-loop potential  $\mathcal{U}$  used here is determined by using the strong coupling expansion of the pure Yang-Mills theory. The logarithmic part comes from the Haar measure. Since the parameter fitting procedure does not refer to microscopic dynamics, it is unclear how the Polyakov-loop potential is related to non-perturbative characteristics near  $T_c$ . This problem should be investigated elsewhere by considering other approach based on gluon and ghost propagators [31].

$m_\pi$ [MeV]	$f_\pi$ [MeV]	$M_0$ [MeV]
140	74.5	305
$G$ [GeV <sup>-2</sup> ]	$\Lambda$ [MeV]	$m$ [MeV]
7.23	657	5.4

TABLE I: Summary of parameters and physical values.

### B. $\theta$ dependence of order parameters

Figures 1(a)-(c) represent  $\theta$  dependence of  $M$ ,  $\text{Im}[\Psi]$  and  $\Phi$ , respectively, for three cases of  $\alpha = 0, 0.2$  and  $0.4$ . Here we consider the high- $T$  case of  $T = 2.5m_\pi$ . Quantities  $M$ ,  $\text{Im}[\Psi]$  and  $\Phi$  are order parameters of the chiral, the  $\mathcal{C}$  and the  $\mathbb{Z}_2$  symmetry, respectively.  $\theta$ -even and  $\mathbb{Z}_2$ -odd quantities such as  $\Phi$  are antisymmetric with respect to the  $\theta = \pi/2$  axis, whereas  $\theta$ -even and  $\mathbb{Z}_2$ -even quantities such as  $M$  are symmetric with respect to the axis. In addition,  $\theta$ -odd and  $\mathbb{Z}_2$ -even quantities such as  $\text{Im}[\Psi]$  are antisymmetric with respect to the  $\theta = \pi/2$  axis and zero at  $\theta = 0$  and  $\pi$ . As shown in panel (b),  $\text{Im}[\Psi]$  has a gap at  $\theta = \pi/2$ , indicating that the  $\mathcal{C}$  symmetry is spontaneously broken there for the high- $T$  case. The zeroth-order discontinuity (gap) in  $\text{Im}[\Psi]$  means that a first-order phase transition takes place at  $\theta = \pi/2$ . This is the RW phase transition [7]. At  $\theta = \pi/2$ ,  $\Phi$  also has a gap, indicating that the  $\mathbb{Z}_2$  symmetry is spontaneously broken there. The  $\mathcal{C}$  and  $\mathbb{Z}_2$  symmetry are always simultaneously broken on the RW phase transition line, since  $\text{Im}[\Psi] = \sin(\theta)\Phi$  and hence  $\text{Im}[\Psi] = \Phi$  at  $\theta = \pi/2$ . This is a characteristic of two-color QCD.

The  $\theta$ -even quantity  $M$  has a cusp at  $\theta = \pi/2$ , when the  $\theta$ -odd quantity  $\text{Im}[\Psi]$  has a gap there. In general, the zeroth-order discontinuity (gap) in a  $\theta$ -odd quantity is propagated to other  $\theta$ -odd quantities as the zeroth-order discontinuity (gap) and to  $\theta$ -even quantities as the first-order discontinuity (cusp) [32, 33]. The order parameters  $\text{Im}[\Psi]$  and  $\Phi$  are less sensitive to  $\alpha$  than  $M$ .

### C. Interplay between chiral and deconfinement transitions

Figure 2 shows  $T$ -dependence of  $M/M_0$  and  $|\Phi|$  at  $\theta = \pi/2$  for three cases of  $\alpha = 0, 0.2$  and  $0.4$ . The decon-

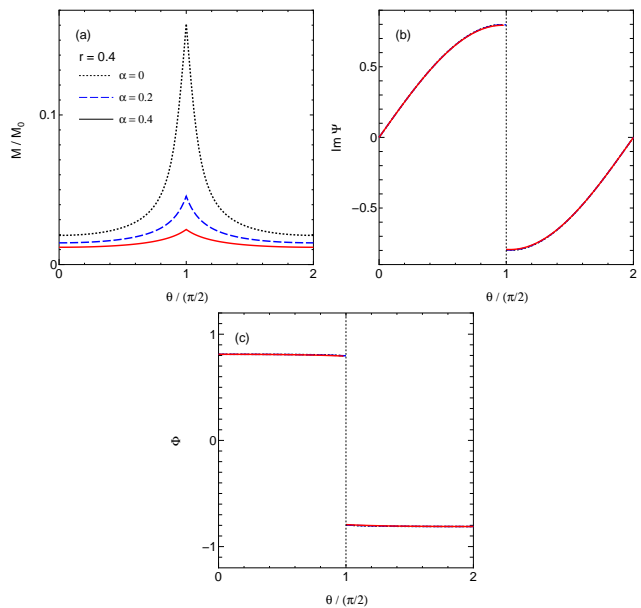


FIG. 1:  $\theta$ -dependence of order parameters  $M$ ,  $\text{Im}[\Psi]$  and  $\Phi$  at  $T = 2.5m_\pi$ . Here  $M$  is normalized by the value  $M_0$  at  $T = \mu = 0$ . The dotted, dashed and solid lines represent the results of  $\alpha = 0, 0.2$  and  $0.4$ , respectively.

finement transition, i.e. the  $\mathbb{Z}_2$ -symmetry breaking transition, is the second order for  $\alpha = 0$  and  $0.2$ , but becomes the first order for  $\alpha = 0.4$ . Here the vertical thin-dotted line denotes the critical temperature  $T_d^c$  of the first-order transition. Since the spontaneous breakings of the  $\mathbb{Z}_2$  and  $\mathcal{C}$  symmetries take place simultaneously, the order of the deconfinement transition is the same as that of the RW transition at the endpoint. The chiral transition is crossover for  $\alpha = 0$  and  $0.2$ , but it becomes the first order for  $\alpha = 0.4$ . Thus the entanglement intensifies both the chiral and deconfinement transitions. For  $\alpha = 0$  and  $0.2$ ,  $M$  has a cusp at  $T = T_d^c$  as a result of the propagation of the first-order discontinuity in  $|\Phi|$  [33].

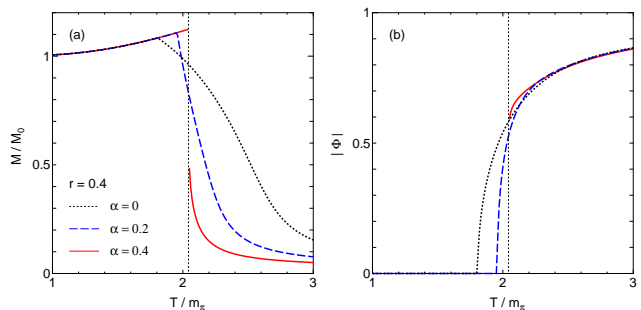


FIG. 2:  $T$ -dependence of (a)  $M/M_0$  and (b)  $|\Phi|$  at  $\theta = \pi/2$ . The dotted, dashed and solid lines represent the results of  $\alpha = 0, 0.2$  and  $0.4$ , respectively.

Figure 3 shows  $T$ -dependence of  $M/M_0$  and  $\Phi$  at  $\theta = 0$

( $\mu = 0$ ). Both the deconfinement and chiral transitions keep crossover for  $\alpha = 0, 0.2$  and  $0.4$ , although the transitions become stronger as  $\alpha$  increases. The pseudo-critical temperature  $T_d^c$  of the deconfinement transition is less sensitive to  $\alpha$  than the pseudo-critical temperature  $T_\chi^c$  of the chiral transition, where the pseudo-critical temperatures are defined by peak positions of  $dM/dT$  and  $d\Phi/dT$ , respectively.

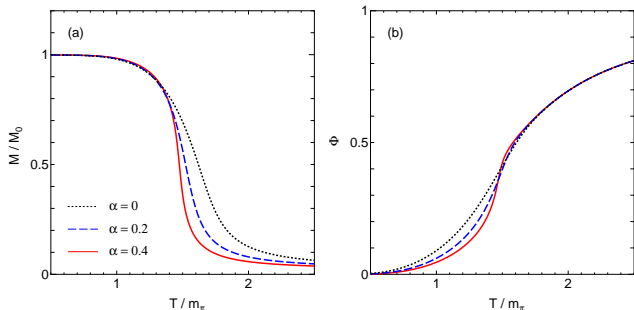


FIG. 3:  $T$ -dependence of (a)  $M/M_0$  and (b)  $\Phi$  at  $\mu = 0$ . See Fig. 2 for the definition of lines.

The system at  $\theta = \pi/2$  has higher symmetries than that at  $\mu = 0$ . Hence the order parameters have discontinuities of either the zeroth or the first order at  $\theta = \pi/2$ . The order parameters are considered to be more sensitive to  $\alpha$  near the discontinuities. This is really true as seen by comparing Fig. 2 with Fig. 3. Through the discontinuities, we can then investigate clearly how strong the entanglement between the chiral and deconfinement transitions is. The symmetry breakings at the lower bound  $\mu^2 = -(T\pi/N_c)^2$  thus give deeper understanding.

Figure 4 shows  $\alpha$ -dependence of two (pseudo)critical temperatures  $T_d^c$  and  $T_\chi^c$  at  $\theta = \pi/2$  and  $0$ . The two (pseudo)critical temperatures approach each other as  $\alpha$  increases, and finally agree with each other at  $\alpha \gtrsim 0.2$  for  $\theta = \pi/2$  and at  $\alpha \gtrsim 0.4$  for  $\theta = 0$ . As for  $\alpha \lesssim 0.2$ , the speed of the approach is much faster for  $\theta = \pi/2$  than for  $\theta = 0$ . The entanglement thus makes it stronger the correlation between the chiral and deconfinement transitions. Therefore, the difference  $|T_\chi^c - T_d^c|$  is a good quantity to determine the value of  $\alpha$ . For  $\theta = \pi/2$ , the deconfinement transition is the second order at  $\alpha < \alpha_c \approx 0.33$ , but the first order at  $\alpha > \alpha_c$ . The chiral transition is, meanwhile, crossover at  $\alpha < \alpha_c$ , although it is the first order at  $\alpha > \alpha_c$ . Hence, the point at  $\alpha = \alpha_c$  is a tri-critical point (TCP) for the deconfinement transition and a critical endpoint for the chiral transition.

Figure 5 shows  $r$ -dependence of  $M/M_0$  and  $|\text{Im } \Psi|$  at  $\theta = \pi/2$ . The effect of  $r$  is similar to that of  $\alpha$ , but the former effect is smaller than the latter one, when  $r$  is varied within a realistic range from  $0.25$  to  $0.5$ .

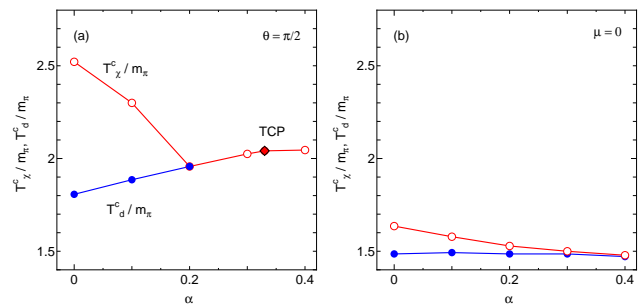


FIG. 4:  $\alpha$ -dependence of (pseudo)critical temperatures  $T_d^c$  and  $T_\chi^c$  at (a)  $\theta = \pi/2$  and (b)  $\mu = 0$  for the case of  $G_v = 0.4G$ . The closed diamond symbols stands for the tri-critical point (TCP). The numerical values have ambiguities of about 1 MeV and the solid lines are drawn by connecting two neighborhood points.

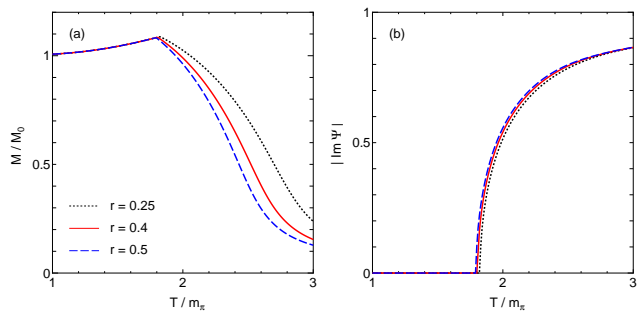


FIG. 5:  $T$ -dependence of (a)  $M/M_0$  and (b)  $|\text{Im } \Psi|$  at  $\theta = \pi/2$ . The dotted, dashed and solid lines denote the results for  $r = 0.25, 0.4$  and  $0.5$ , respectively. Here  $\alpha$  is set to  $0.4$ .

#### D. Phase diagram at imaginary and real chemical potentials

First we consider the phase diagram at imaginary  $\mu$  for two cases of  $\alpha = 0$  and  $0.4$ . Here we take  $r = 0.4$ . Figure 6 shows the phase diagram in the  $\theta$ - $T$  plane. In the left panel for the case of  $\alpha = 0$ , the upper and lower dotted lines denote chiral and deconfinement crossover transitions, respectively. The two transitions are thus separated from each other, when the correlation between the two transitions is weak. In this situation, the  $\mathcal{C}$  symmetry breaking at the RW endpoint is the second order. In the right panel for the strong correlation case of  $\alpha = 0.4$ , the two crossover transitions (dotted lines) agree with each other and the  $\mathcal{C}$  symmetry breaking at the RW endpoint becomes the first order. In other words, the RW endpoint becomes a triple-point where three first-order transition lines meet. Thus, the RW endpoint becomes a triple-point, when the correlation between the chiral and deconfinement transition are strong.

The Polyakov-loop potential used in this study yields the second-order  $\mathbb{Z}_2$  symmetry breaking in the heavy quark limit. Since the entanglement parameter  $\alpha$  makes

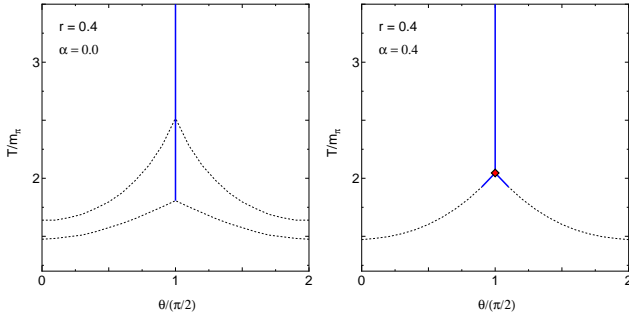


FIG. 6: The phase diagram in the  $\theta$ - $T$  plane for  $\alpha = 0$  (left panel) and (b)  $\alpha = 0.4$  (right panel). Here the case of  $r = 0.4$  is taken. The dotted and solid lines stand for crossover and first-order transitions, respectively. In the left panel, the upper and lower dotted lines mean the chiral and deconfinement crossover lines, respectively. In the right panel, the chiral and deconfinement crossover lines almost coincide with each other, and the diamond symbol denotes the triple-point.

the symmetry breaking stronger, the first-order  $\mathbb{Z}_2$  symmetry breaking in the physical quark mass does not come from the  $\mathbb{Z}_2$  symmetry breaking only. The chiral transition becomes stronger, if the coupling constant  $G$  is weakened at finite  $T$ ; see for example Ref. [34]. In the present model, the coupling constant is weakened through the entanglement vertex, so that the chiral transition becomes the first-order. This behavior is seen in the left panel of Fig. 2. Therefore, the first-order  $\mathbb{Z}_2$  symmetry breaking is induced by the first-order chiral transition.

Next we investigate an influence of  $\alpha$  on the phase diagram at real  $\mu$ . Figure 7 shows  $T$ -dependence of  $M/M_0$ ,  $\Phi$ ,  $\Delta/\sigma_0$  and  $n_q$  for the case of  $r = 0.4$  and  $\mu = m_\pi$ , where  $\sigma_0$  is the absolute value of  $\sigma$  at  $T = \mu = 0$ . As shown in panel (c),  $\Delta/\sigma_0$  vanishes around  $T = 1.5m_\pi$ , indicating that the superfluid/normal transition occurs there. The phase boundary is rather sensitive to  $\alpha$ .

In this study, we take  $r \equiv G_v/G = 0.4$  for all the calculations. Although this value is obtained from the  $N_c = 3$  case by comparing the PNJL results with the corresponding LQCD data, it is not easy to determine the value definitely. We then check  $r$ -dependence of order parameters, as shown in Fig. 8 where  $r = 0.25$  and  $0.5$  are taken as lower and upper limits of a reliable range of  $r$ . Effects of  $r$  on  $M$ ,  $\Phi$  and  $\Delta$  are rather small, although  $r$  gives an appreciable effect on  $n_q$ .

Finally we consider the phase diagram at real  $\mu$ . Figure 9 shows the BCS-BEC crossover ( $M = \mu$ ), the deconfinement crossover ( $\Phi = 0.5$ ) and the superfluid/normal transition lines for two cases of  $\alpha = 0$  and  $0.4$ ; see Ref. [28] for the definitions of these transitions. When  $T$  is small, the superfluid/normal transition occurs at  $\mu = m_\pi/2$  as expected. When  $T > m_\pi$  and  $\mu > m_\pi/2$ , meanwhile, the superfluid/normal transition takes place around  $T = 1.5m_\pi$ . The transition line depends on  $\alpha$  rather strongly compared with the BCS-BEC crossover

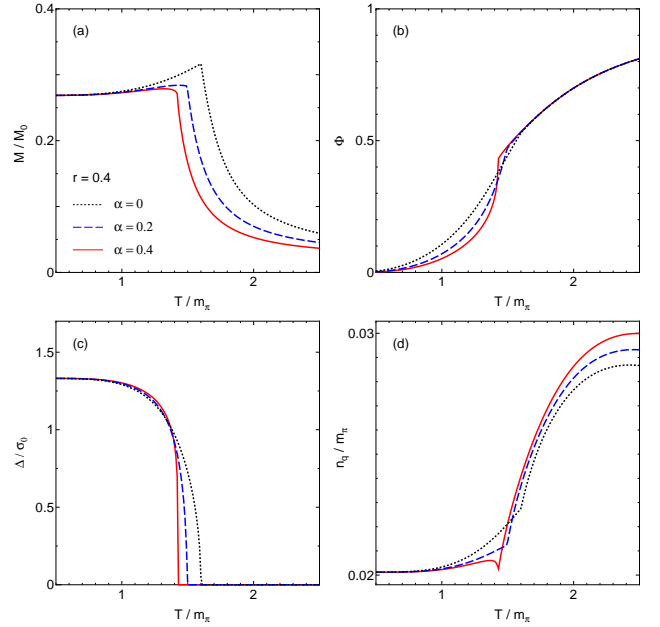


FIG. 7:  $T$ -dependence of (a)  $M/M_0$ , (b)  $\Phi$ , (c)  $\Delta/\sigma_0$  and (d)  $n_q$  for the case of  $r = 0.4$  and  $\mu = m_\pi$ . The dotted and solid lines represent the results of  $\alpha = 0$  and  $0.4$ , respectively.

and the deconfinement crossover line. Thus the correlation between the chiral and deconfinement transitions is important not only at the lower bound  $\mu^2 = -(T\pi/2)^2$  but also at large real  $\mu$  such as  $\mu^2 > (m_\pi/2)^2$ .

## V. SUMMARY

We have studied properties of two-color QCD at imaginary  $\mu$  from the view point of the RW periodicity, the charge conjugation and the pseudo-reality. The parameter  $\mu^2$  has a lower bound:  $\mu^2 \geq -(\pi T/2)^2$ . At the lower bound, the system has higher symmetries, that is, the  $\mathbb{Z}_2$  and  $\mathcal{C}$  symmetries. These symmetries are simultaneously broken, since their order parameters,  $\Phi$  and  $\text{Im}[\Psi]$ , are identical in virtue of the pseudo-reality. The pseudo-reality also guarantees that the  $1+1$  system with finite  $\mu$  is identical with the  $1+1^*$  system with the same amount of isospin chemical potential  $\mu_{iso}$ , so that  $\mu_{iso}^2$  has a lower bound:  $\mu_{iso}^2 \geq -(\pi T/2)^2$ .

The PNJL model has the same properties as two-color QCD for the RW periodicity, the charge conjugation and the pseudo-reality. The PNJL model is thus a good model to investigate two-color QCD at imaginary  $\mu$  concretely. We have then investigated the nontrivial correlation between the deconfinement and chiral transitions at imaginary  $\mu$  for the two-flavor case. The Polyakov loop as an order parameter of the deconfinement transition is  $\mathbb{Z}_2$ -odd and  $\mathcal{C}$ -even ( $\theta$ -even), while the chiral condensate as an order parameter of the chiral transition is  $\mathbb{Z}_2$ -even and  $\mathcal{C}$ -even. The order parameters are thus different  $\theta$ -de-

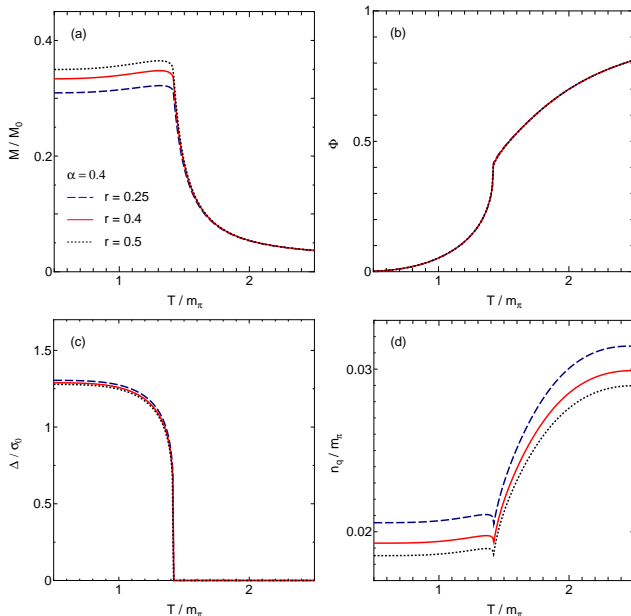


FIG. 8:  $T$ -dependence of (a)  $M/M_0$ , (b)  $\Phi$ , (c)  $\Delta/\sigma_0$  and (d)  $n_q$  for the case of  $\alpha = 0.4$  and  $\mu = m_\pi$ . The dotted, solid and dashed lines represent the results of  $r = 0.25, 0.4$  and  $0.5$ , respectively.

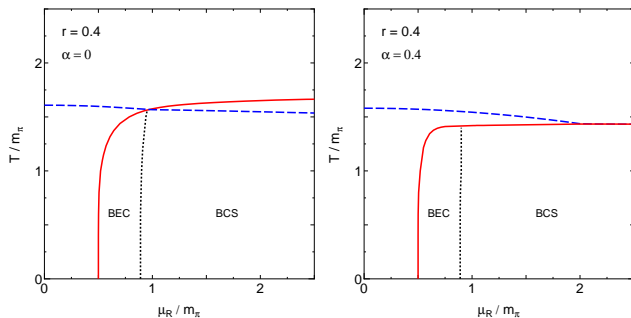


FIG. 9: The phase diagram in the  $\mu$ - $T$  plane for  $\alpha = 0$  (left panel) and  $0.4$  (right panel). Here the case of  $r = 0.4$  is taken. The dotted, dashed and solid lines stand for the BCS-BEC crossover ( $M = \mu$ ), the deconfinement crossover ( $\Phi = 0.5$ ) and the superfluid/normal transition lines, respectively.

pendence. At  $\theta = \pi/2$ , the simultaneous breaking of  $\mathbb{Z}_2$  and  $\mathcal{C}$  symmetries takes place at higher  $T$ , and the breaking is induced by the RW phase transition. The order of the  $\mathbb{Z}_2$  and  $\mathcal{C}$  symmetry breakings at the RW endpoint is nontrivial. It cannot be determined by the  $\mathbb{Z}_2$  and  $\mathcal{C}$  symmetries and the pseudo-reality. The order depends on the strength of the entanglement parameter  $\alpha$ , i.e., the strength of the correlation between the chiral and  $\mathbb{Z}_2$  symmetry breakings. The order is the second-order for small  $\alpha$ , but becomes the first-order for large  $\alpha$ . The second-order nature is originated in the Polyakov potential. Meanwhile, the first-order nature comes from the fact that the chiral symmetry breaking becomes the first order as a consequence of the strong entanglement. The order of the  $\mathbb{Z}_2$  and  $\mathcal{C}$  symmetry breakings at the RW endpoint is thus sensitive to the strength of the correlation between the chiral and  $\mathbb{Z}_2$  symmetry breakings. Finally, we have investigated the impact of  $\alpha$  on the phase diagram at real  $\mu$ . The diagram, particularly the superfluid transition, is rather sensitive to  $\alpha$ . The determination of  $\alpha$  is thus important for both real and imaginary  $\mu$ .

At the present stage, we do not know how large  $\alpha$  is, but it is possible to determine the value of  $\alpha$  from LQCD simulations at  $\theta = \pi/2$ , particularly by seeing the correlation between the chiral and  $\mathbb{Z}_2$  symmetry breakings. It is interesting as a future work. In two-color QCD, the correlation between the chiral and deconfinement transitions is thus important for both real and imaginary  $\mu$ . This is true also for three-color QCD. This strongly suggests that understanding of three-color QCD at imaginary  $\mu$  is important to determine the phase diagram at real  $\mu$ .

## Acknowledgments

K.K. is supported by RIKEN Special Postdoctoral Researchers Program. T.S. is supported by JSPS.

[1] P. de Forcrand, PoS (LAT2009) p. 010 (2009), 1005.0539.  
[2] K. Fukushima, Phys. Lett. **B591**, 277 (2004), hep-ph/0310121.  
[3] C. Ratti, M. A. Thaler, and W. Weise, Phys. Rev. D **73**, 014019 (2006), hep-ph/0506234.  
[4] Y. Sakai, K. Kashiwa, H. Kouno, and M. Yahiro, Phys. Rev. D **77**, 051901 (2008), 0801.0034.  
[5] T. Hell, S. Roessner, M. Cristoforetti, and W. Weise, Phys. Rev. D **79**, 014022 (2009), 0810.1099.  
[6] K. Kashiwa, T. Hell, and W. Weise, Phys. Rev. D **84**, 056010 (2011), 1106.5025.

[7] A. Roberge and N. Weiss, Nucl. Phys. **B275**, 734 (1986).  
[8] H. Kouno, Y. Sakai, K. Kashiwa, and M. Yahiro, J. Phys. G **36**, 115010 (2009), 0904.0925.  
[9] M. D'Elia and F. Sanfilippo, Phys. Rev. D **80**, 111501(R) (2009), 0909.0254.  
[10] C. Bonati, G. Cossu, M. D'Elia, and F. Sanfilippo, Phys. Rev. D **83**, 054505 (2011), 1011.4515.  
[11] P. de Forcrand and O. Philipsen, Phys. Rev. Lett. **105**, 152001 (2010), 1004.3144.  
[12] C. Bonati, P. de Forcrand, M. D'Elia, O. Philipsen, and F. Sanfilippo (2012), 1201.2769.



- [13] Y. Sakai, H. Kouno, and M. Yahiro, *J. Phys.* **G37**, 105007 (2010), 0908.3088.
- [14] Y. Sakai, T. Sasaki, H. Kouno, and M. Yahiro, *Phys.Rev.* **D82**, 076003 (2010), 1006.3648.
- [15] T. Sasaki, Y. Sakai, H. Kouno, and M. Yahiro, *Phys. Rev. D* **84**, 091901 (2011), 1105.3959.
- [16] J. B. Kogut, M. A. Stephanov, D. Toublan, J. J. M. Verbaarschot, and A. Zhitnitsky, *Nucl.Phys.* **B582**, 477 (2000), hep-lat/0001171.
- [17] E. Witten, *Nucl. Phys.* **B160**, 57 (1979).
- [18] J. M. Maldacena, *Adv. Theor. Math. Phys.* **2**, 231 (1998).
- [19] J. B. Kogut, D. K. Sinclair, S. J. Hands, and S. E. Morrison, *Phys. Rev.* **D64**, 094505 (2001), hep-lat/0105026.
- [20] P. Giudice and A. Papa, *Phys. Rev. D* **69**, 094509 (2004), hep-lat/0401024.
- [21] P. Cea, L. Cosmai, M. D’Elia, and A. Papa, *JHEP* **0702**, 066 (2007), hep-lat/0612018.
- [22] P. Cea, L. Cosmai, M. D’Elia, and A. Papa, *PoSLAT2007* p. 214 (2007), 0710.2068.
- [23] P. Cea, L. Cosmai, M. D’Elia, and A. Papa, *Phys. Rev. D* **77**, 051501 (2008), 0712.3755.
- [24] P. Cea, L. Cosmai, M. D’Elia, and A. Papa, *Nucl. Phys.* **A820**, 239c (2009), 0812.2777.
- [25] P. Cea, L. Cosmai, M. D’Elia, C. Manneschi, and A. Papa, *Phys. Rev. D* **80**, 034501 (2009), 0905.1292.
- [26] W. Pauli, *Nuovo Cimento* **6**, 205 (1957).
- [27] W. Pauli, *ibid* **7**, 411 (1958).
- [28] T. Brauner, K. Fukushima, and Y. Hidaka, *Phys. Rev. D* **80**, 074035 (2009), 0907.4905.
- [29] K.-I. Kondo, *Phys. Rev. D* **82**, 065024 (2010), 1005.0314.
- [30] T. Hell, K. Kashiwa, and W. Weise, *Phys. Rev. D* **83**, 114008 (2011), 1104.0572.
- [31] K. Fukushima and K. Kashiwa (2012), 1206.0685.
- [32] A. Barducci, R. Casalbuoni, G. Pettini, and R. Gatto, *Phys. Lett.* **B301**, 95 (1993), hep-ph/9212276.
- [33] K. Kashiwa, M. Yahiro, H. Kouno, M. Matsuzaki, and Y. Sakai, *J. Phys.* **G36**, 105001 (2009), 0804.3557.
- [34] K. Kashiwa, H. Kouno, T. Sakaguchi, M. Matsuzaki, and M. Yahiro, *Phys. Lett.* **B647**, 446 (2007), 0608078.